

Chitosan Modified by Polymeric Reactive Dyes Containing Quaternary Ammonium Groups as a Novel Anion Exchange Membrane for Alkaline Fuel Cells

Tianchi Zhou, Xuemei He, Feifei Song, Kongliang Xie*

¹College of Chemistry, Chemical Engineering and Biotechnology, Donghua University, 2999 Ren'min North Road, Shanghai 201620, China

²YanCheng Institute of Technology, 9 Ying'bing Road, Yancheng 224051, China

³College of Environmental Science and Engineering, Donghua University, 2999 Ren'min North Road, Shanghai 201620, China

*E-mail: 120413181@qq.com

Received: 24 September 2015 / Accepted: 7 November 2015 / Published: 1 December 2015

A new type of anion exchange membranes based on Chitosan (CTS) modified by polymeric reactive dyes containing quaternary ammonium groups (PRDQA) has been prepared and evaluated as OH^- conducting polymer electrolytes. The effect of the content of PRDQA on membrane OH^- conductivity and water uptake was studied using AC impedance technique and weighing method, respectively. FTIR and SEM were used for chemical and structural characterization of the membranes. The CTS/PRDQA membrane (1:0.5 in mass) exhibited a high OH^- conductivity of $8.17 \times 10^{-3} S cm^{-1}$ at room temperature. At a current density of $57.4 mA cm^{-2}$, this membrane achieved a power density of $29.1 mW cm^{-2}$ with an open-circuit voltage (OCV) of 991.6mV in a H_2/O_2 system. Compared to the pristine CTS membrane, this membrane also demonstrated a good stability after one week testing in the 8.0M of KOH solution at 80°C in terms of both integrity and OH^- conductivity.

Keywords: membrane; polymeric reactive dyes; conductivity; thermal stability; modification

1. INTRODUCTION

In general, low temperature PEM fuel cells (normally < 90°C) can be classified into two categories: one is alkaline fuel cell, the other is acidic fuel cell [1-3]. The membranes used in alkaline PEM fuel cells conduct hydroxide ions (OH^-) [4], while acidic membranes conduct protons (H^+) [5]. At present, acidic membranes (such as Nafion[®]) are mainly used in the low temperature PEM fuel cells due to their mechanical stabilities and high conductivity at ambient temperature [6]. Unfortunately,

some challenges such as high cost, low stability at high temperatures, the potential health or environmental issues as well as the difficulties in the synthesis and processing narrow its wide applications [7,8].

Recently, alkaline PEM fuel cells have attracted significant attention due to several promising advantages over acidic PEM fuel cells such as: 1) a faster oxygen reduction reaction, which allows the use of cost-effective non-Pt-based catalysts [9-12]; 2) a less corrosive environment, which makes the inexpensive component materials possible [13]; 3) a slower fuel crossover rate, which [14] allows the possibility of using low-cost materials [15-17]; 4) a better water management [18]. Although alkaline PEM fuel cells have shown some promising advantages, several challenges still remain [19] such as: 1) insufficient membrane ionic conductivity; 2) high membrane resistance; 3) lower mechanical and chemical stability; 4) CO₂ poisoning; and 5) water-related issues.

To solve these problems, some new alkaline membranes (AAEMs) have been developed, where the membranes are constructed mainly by two parts: one part is the polymer that serves as the matrix; the other part is the OH⁻-conductive functional groups, such as the quaternary ammonium cationic groups that are introduced to the main chains or side chains of the polymer matrixes. Some polymers, such as poly(vinylidene fluoride) (PVDF) [20], poly(ethylene-co-tetrafluoroethylene) (ETFE) [21], poly(ethersulfone cardo) [22], poly(2,6-dimethyl-1,4-phenyleneoxide) (PPO) [23], poly(tetrafluoroethylene-co-hexafluoropropylene) (FEP) [24], poly(tetrafluoroethylene-co-perfluoropropyl vinyl ether) (PFA) [25], polyethylene including low-density polyethylene (LDPE) [26], high-density polyethylene (HDPE) [27] and ultra-high molecular weight polyethylene (UHMWPE) [28], polyvinyl alcohol (PVA) [4,29,30], polysulfone (PSO) [31,32], polyvinyl chloride (PVC) [33], have been chosen to prepare membranes. Hu et al. [33] prepared a P1NOH based on PVC membrane with a ionic conductivity of 0.0145 S cm⁻¹ at 20°C, however, the power density was 1.4 mW cm⁻² in the air breathing fuel cell using 2M ethanol at room temperature. Zhang et al. [30] prepared a series of cross-linked PVA/PDDA based membranes, which showed high ionic conductivity up to 0.027 S cm⁻¹, but the membrane stability was poor due to the lost of PDDA during the period of use. Danks et al. [20] used PVDF, vinylbenzyl chloride (VBC) and trimethylamine (TMA) to construct a novel anion exchange membrane using radiation grafting technology, but the mechanical properties of the membrane were not good due to the main chain's deterioration. Furthermore, these polymers are generally synthetic macromolecules that need an extra energy to prepare. In addition, the production processes of the corresponding anion exchange membranes are often complex, expensive and harmful to the environment [19]. Furthermore, the quaternary ammonia groups in these membranes can be removed under the condition of high temperature and concentrated alkali solutions through either an E₂ Hofmann elimination or an SN₂ substitution reaction [34,35]. Hence it is urgent to develop cost-effective, environmentally friendly and alkaline stable membranes.

In this work, we prepared a novel alkaline anion-exchange membrane based on chitosan (CTS) and polymeric reactive dyes containing quaternary ammonium groups (PRDQA). The conductivity and alkaline stability of the obtained membranes are comparable to that of Tokuyama A901. Natural polymer CTS, the (1-4)-2-amino-2-deoxy-D-glucan, has attracted great attention in the membrane preparation due to its excellent film forming characteristics, biodegradability, alkaline stability, high water holding capacity, good mechanical and thermal property, low cost, environmental friendly, high

contents of amino and hydroxyl functional groups for cross-linking or grafting in the chains [36,37]. However, few studies of CTS on the fuel cell application are found since CTS is sensitive to acid. This issue can be addressed in alkaline anion exchange membrane fuel cells due to the alkaline stability of CTS. Polymeric reactive dyes have been widely used in photoelectric material, biomedical, textile dyeing and some other fields since it was firstly synthesized in 1970s. Polymeric reactive dyes have many advantages such as spectrally selecting absorption, good stability, hypotoxicity and biocompatibility of high molecular polymer [38]. In this work, polymeric dyes containing quaternary ammonium groups were synthesized with a home-made reactive dye and polyethylenimine (PEI) (Shanghai Gongbike Co.,Ltd, China). After blending and dyeing, PRDQA can be firmly fixed on the CTS matrix since the chlorotriazinyl groups (grafted onto the main chain of PEI) could react with CTS to form covalent bonds. Since PRDQA is a quaternized polymer, it can offer quaternary ammonium groups as charge carriers to conduct hydroxide. Furthermore, the two polymer components can form interpenetrating polymer networks in which the charge carriers can better reside and the quaternized ammonium can be better protected.

On the basis of above designs, a series of CTS/PRDQA composite membranes were prepared through blending and dyeing processes. The membranes thus prepared were investigated by infrared spectroscopy (FT-IR) and scanning electron microscope (SEM) for chemical structure and morphological microstructure analysis. Thermogravimetric analysis (TGA) was used for thermal stability of the membranes. The membrane characteristics including OH^- conductivity (σ), water uptakes (WU) and alkaline stabilities were discussed for performance evaluation. , the obtained CTS/PRDQA membranes (1:0.5 in mass) were used for membrane electrode assemblies (MEAs) construction and tested in a H_2/O_2 single fuel cell.

2. EXPERIMENTAL

2.1 Synthesis of PRDQA

The synthetic process of PRDQA(Figure.1) was divided into 4 steps:

Firstly, 300mL of nitrobenzene was added into a 500mL of three-necked flask as the reactive solvent. After the solvent was heated up to 90°C, 22.4g of 1-amino-anthraquinone and 27.68g of cyanuric chloride were added into it and mixed well by a magnetic stirrer. The solution temperature was controlled around 90°C under refluxing for 1h, and then it was heated up further to 120°C and kept at this temperature until the reaction was complete. Thin Layer Chromatography (TLC) (ethyl acetate: petroleum ether =1:5, v/v) was used to identify whether the reaction was complete. Then the reaction mixture was cooled down slowly to 40°C followed by a filtration to get the crude product. After several times of washing with petroleum ether, acetone and alcohol, the filter cake was dried in a vacuum oven. Finally, the earthy yellow solid LRD product was collected for further use.

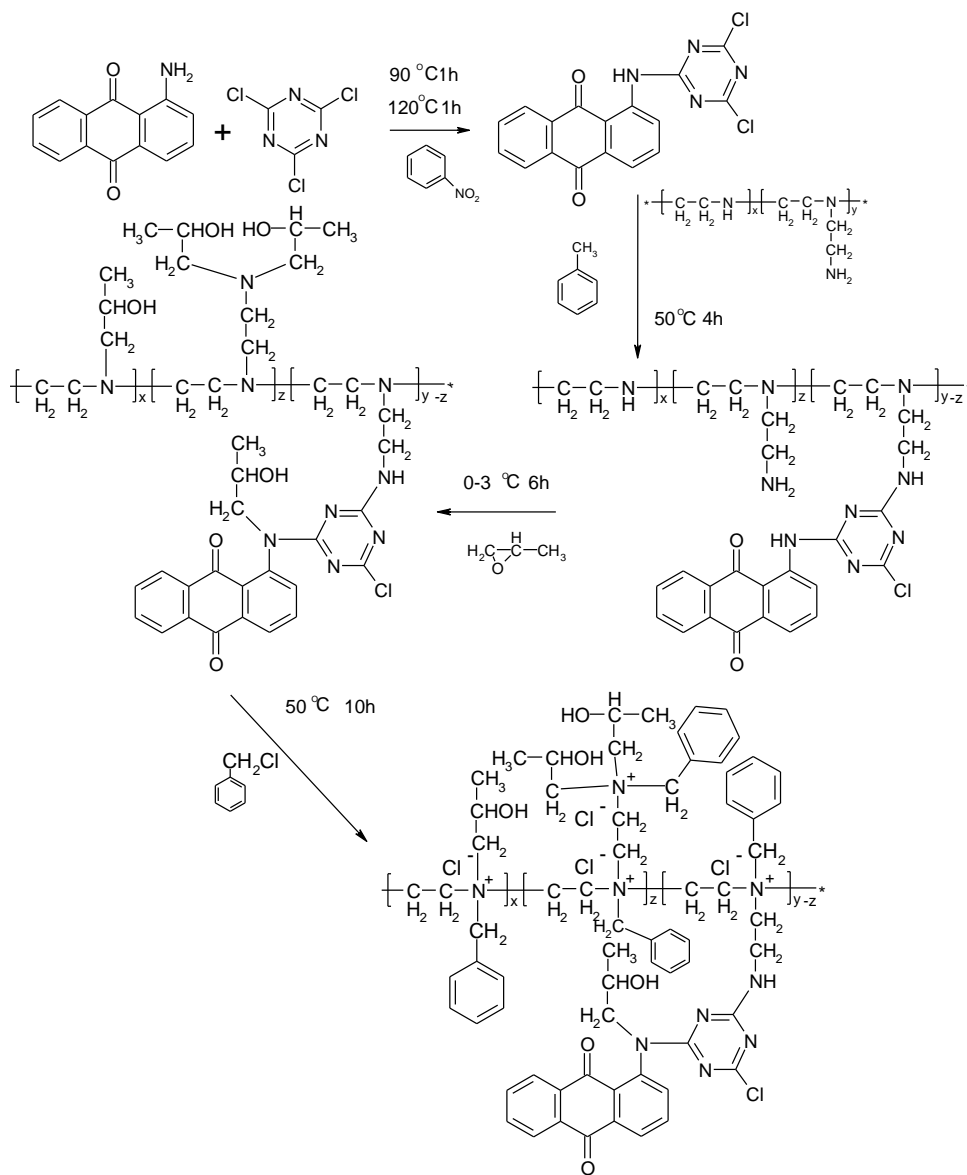


Figure 1. The whole reaction equation of synthesis PRDQA.

Secondly, 4g of LRD, 15.8g of PEI, 2mL of triethylamine and a mixed solvent composed of 10mL of deionized water and 50mL of methylbenzene were put into a 250mL of three-necked flask and mixed thoroughly. After reaction at 65°C for 5h, the reaction product was treated by reduced pressure distillation to remove triethylamine and methylbenzene. Thus a yellow-brown and viscous intermediate PRD product was obtained.

Thirdly, 100mL of PRD solution (10g/L) was added into a 250mL of three-necked flask followed by 1.22g of epoxypropane into the same flask through a dropping funnel. After dripping out the liquid, the system temperature was controlled in the range of 0-3°C for 6h. Then the reaction product of PRDE was treated by reduced pressure distillation to remove unreacted epoxypropane.

Finally, 100mL of PRDE solution (8g/L) and 0.21g of benzyl chloride were added into a 250mL of three-necked flask followed by a mixture by a magnetic stirrer at 50°C for 10h. After reaction, the solution of PRDQA was obtained through extraction with diethyl ether to remove the

trace amounts of benzyl chloride in the aqueous phase. The yellow-brown and viscous PRDQA was precipitated out with acetone followed by washing with ethanol and acetone. This was further dried in a vacuum oven at 40°C until a constant weight product was obtained.

2.2 Membrane preparation

A chitosan (degree of deacetylation 96.31%, MW = 7.9×10^5 Da, Zhejiang Jinke Bio-tech Co., Ltd, China) aqueous solution was prepared by dissolving CTS in a 1% acetic acid solution at room temperature overnight. Home-made PRDQA was prepared into solutions with various concentrations, and then mixed with the above CTS solution under stirring for at least 60min to ensure a homogeneous solution was obtained.

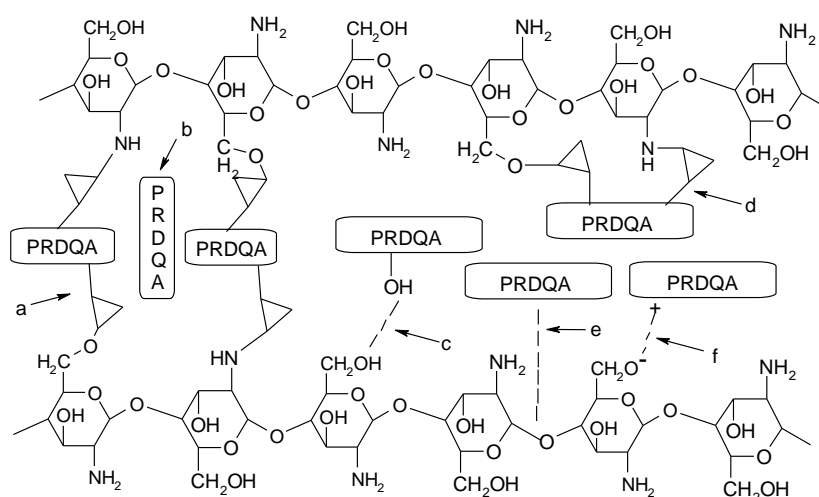


Figure 2. Inner structure of the CTS/PRDQA alkaline exchange membrane. a. crosslinking, b. doping, c. hydrogen bonds, d. grafting, e. Van der Waals forces, f. electrostatic forces.

The obtained solution was heated at 80°C in a water-bath for 2 hours for the completion of the chemical reaction between CTS and PRDQA. The solution was further degassed in a vacuum chamber and transferred into the plastic dishes for drying in an ambient condition. Then the membranes were peeled away from the plastic dishes, immersed into a 1M of NaOH solution for 5min, washed with soap water (5g/L soap flakes)) and then thoroughly rinsed by the tap water to remove unstable color before they were dried naturally. The structure of the CTS/PRDQA membrane is given in Figure.2.

2.3 Membrane characterizations

The molecular structure of membranes was characterized by Fourier transform infrared (FTIR) spectroscopy. The infrared spectrometer (Tensor27,Bucker) equipped with attenuated total reflectance (ATR) instrument was used to obtain the spectrogram in the range from 4000 to 600 cm^{-1} .

The composite morphology was investigated using an FEI Sirion 200 field-emission scanning electron microscope (SEM). The membrane samples were fractured in liquid nitrogen and sputtered with gold, then examined at 10K magnification.

The gravimetric analysis (TGA) of membranes was carried out with a TG 209 analyzer (Netzsch). 5mg of sample was loaded into the alumina pan and heated from 25 to 650°C at a heating rate of 10°C min⁻¹ in an air atmosphere.

Tensile strength (TS, Mpa) and Elongation at break (E_b, %) were measured on a universal material testing machine (H5K-S, Hounsfield) under ambient conditions (room temperature, ~65% relative humidity) at a speed of 12mm min⁻¹ with a 5000 N sensor loaded. The mean value was obtained from at least five strip samples with the size of about 1×5cm.

2.4 The ion exchange capacity

The ion exchange capacity (IEC, mequiv g⁻¹) of the CTS/PRDQA membranes was determined by a titration method. Square pieces of the membranes were first soaked into a 1.0M of KOH solution at room temperature for 24h to obtain the OH⁻ form, and then they were washed with D.I. water to remove any excess of KOH, followed by a drying process in a vacuum oven at 100°C until a constant weight (W_{dry}) was achieved. The obtained samples were eventually equilibrated with a 25mL of 0.1M HCl solution for 24h. The IEC value was determined according to the reduction in acid measured by back titration and was calculated as the ratio of exchangeable hydroxide ions to the weight of dried sample, via the following formula:

$$\text{IEC}(\text{mequiv g}^{-1}) = (N_{\text{O,HCl}} - N_{\text{E,HCl}}) / W_{\text{dry}}$$

where N_{O,HCl} is the HCl quantity (equivalent) in the initial solution, N_{E,HCl} is the remaining amount of HCl (equivalent) determined by the titration, and W_{dry} is the weight of dried membrane.

2.5 OH⁻ conductivity measurement

The OH⁻ conductivity of the obtained membrane was measured by a Zahner Zennium electrochemical AC impedance analyzer, where the AC frequency was scanned from 1MHz to 0.1 Hz at a voltage amplitude of 50mV. Fully hydrated membranes were sandwiched in a Teflon conductivity cell equipped with Pt foil contact on which Pt black was plated. The membrane was in contact with water throughout the measurement. The ionic conductivity (S cm⁻¹), was calculated according to the following equation:

$$\sigma = l / (RA)$$

where *l* and *A* are the thickness and the contact area of the membrane sample, respectively, and *R* is the membrane's resistance.

2.6 Water uptake and Swelling ratio

The swelling of the membranes was evaluated by the water uptake (g g⁻¹) of the membranes. A dry membrane was swelled in D.I. water at room temperature for one day, then the surface water was

wiped carefully with a filter paper, and it was immediately weighed. After drying the sample to a constant weight in a vacuum oven at 100°C, the water uptake was calculated using the following expression:

$$WU = (W_{\text{wet}} - W_{\text{dry}})/W_{\text{dry}}$$

where W_{wet} and W_{dry} are the masses of the fully hydrated membrane and the dry membrane, respectively.

The swelling ratio was measured by immersing the membranes in the deionized water at a constant temperature for one day. The surface water was carefully wiped out, and then the membrane sample was quickly measured to get the values of length (L_x), width (L_y) and thickness (L_z). After drying the sample to a constant weight at 100°C, the same measurement was repeated, thus the swelling ratio (SR) of the membrane was calculated using the following equations:

$$S = L_x \times L_y$$

$$V = L_x \times L_y \times L_z$$

$$\text{Area SR} = (S_{\text{wet}} - S_{\text{dry}})/S_{\text{dry}}$$

$$\text{Volume SR} = (V_{\text{wet}} - V_{\text{dry}})/V_{\text{dry}}$$

where S_{wet} and S_{dry} , V_{wet} and V_{dry} are the area and volume of the fully hydrated membrane and the dry membrane, respectively.

2.7 Alkaline resistance stability

The alkaline resistance of the membranes was evaluated by immersing the membranes into hot KOH (8M) at 80°C for one week. The change of OH^- conductivity of the membranes was measured by AC impedance at certain time intervals. After complete removal of the free KOH from the membrane surface, the OH^- conductivity of the membranes was determined at ambient temperature. The change in water uptake of the membranes was also measured after KOH conditioning.

2.8 Membrane electrode assembly (MEA) fabrication and single-cell performance

The catalyst ink was prepared by mixing 40% of Pt/C (Johnson Matthey) with a solution of 5 wt% Nafion (DuPont) and isopropanol, and then sonicated for 4 h to get a homogeneous solution, where the ratio of Pt/C catalyst to Nafion was 3:1 in weight. Then the catalyst ink was sprayed onto the carbon paper (Toray TGP-H-090) to form a catalyst layer with a Pt loading of 0.5 mg cm⁻² for both the anode and the cathode, respectively. Thenceforth, a few drops of alkaline binder, Tokuyama AS-4, were loaded on the catalyst layers.

The MEA was fabricated by hot-pressing the CTS/PRDQA membrane with the catalyst coated carbon paper at a pressure of 4MPa at 40°C for 4 min. The MEA was tested in a single fuel cell with an active area of 4cm² in a H₂/O₂ feed gas using an electronic load. Pure hydrogen and oxygen were supplied to both the anode and cathode channels at a flow rate of 100 and 70 mL min⁻¹, respectively, through a humidifier at 25°C under ambient pressure. Polarization curves were obtained using a fuel cell evaluation system (GE/FC1-100).

3. RESULTS AND DISCUSSION

3.1 FT-IR studies

Infrared spectra of the pristine CTS membrane as well as the CTS/PRDQA membrane (1:0.5 in mass) are shown in Figure.3.

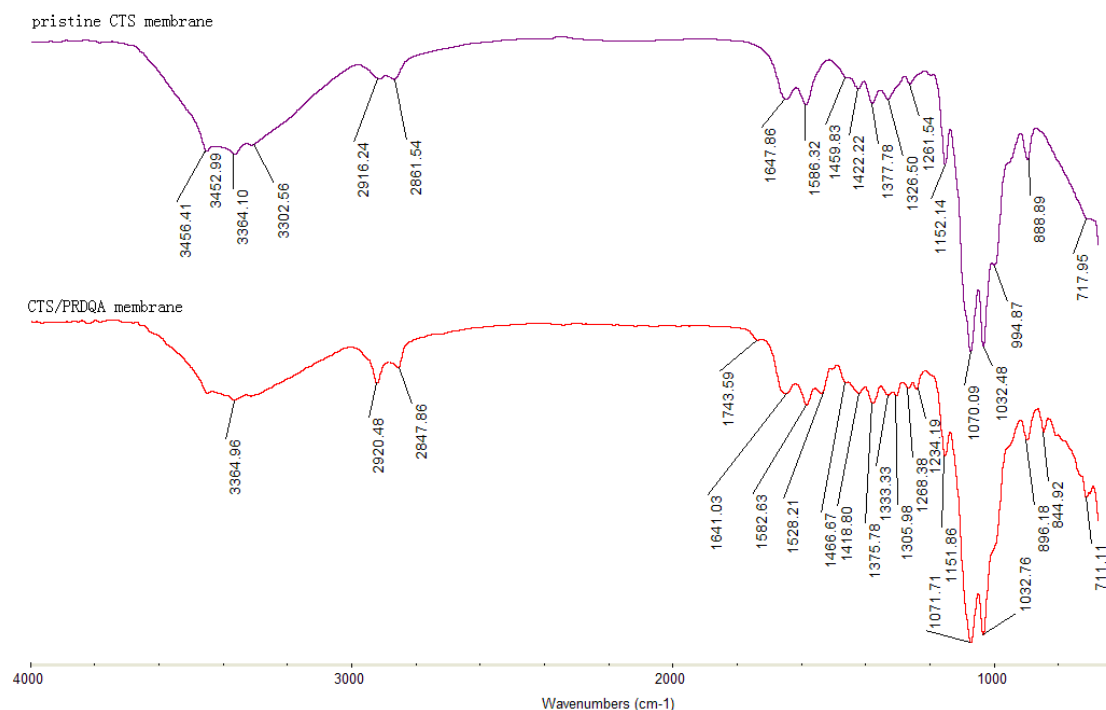


Figure 3. FTIR spectra of the pristine CTS and CTS/PRDQA membrane.

It can be clearly observed for both CTS and PRDQA that the strong absorption peaks between 3000 and 3600 cm^{-1} are ascribed to the stretching vibration of -OH groups and -NH- groups. The bands between 2840 and 2930 cm^{-1} are arisen from the stretching of saturated C-H groups. Compared to the pristine CTS membrane, these characteristic peaks of the CTS/PRDQA membrane show small but significant changes. The appearance of the peaks at 1743 cm^{-1} and 1528 cm^{-1} are assigned to the stretching of carbonyl groups from the quinine structure of PRDQA and the vibration of C=N groups of triazine, indicating that PRDQA was successfully incorporated into the polymer matrix. The appearance of the peak centered at 1305 cm^{-1} may be arisen from the vibration of C-N of secondary and tertiary amines; the peak at 1234 cm^{-1} might be related to =C-O-C in the CTS/PRDQA membrane; the peaks between 700 cm^{-1} and 860 cm^{-1} may be caused by the out-of-plane bending vibration of aromatic rings; and the peaks at 3456 cm^{-1} /3452 cm^{-1} in the CTS/PRDQA membrane that correspond to -NH₂ stretching vibration become weaker compared to those of the pristine CTS membrane. These may illustrate that PRDQA was successfully incorporated into the polymer matrix through chemical reactions. Furthermore, the characteristic peak related to the N-H bands at 1586 cm^{-1} in the pristine

CTS membrane shifts to 1582 cm^{-1} in the CTS/PRDQA membrane, suggesting the existence of intermolecular hydrogen bonds between CTS and PRDQA. The results show that PRDQA was successfully incorporated into the CTS polymer matrix, which may introduce quaternary ammonium cationic groups into the membrane to provide good electrical conductivity.

3.2 The morphology of the pristine CTS membrane and the CTS/PRDQA membrane

As we can see in Figure.4, the pristine CTS membrane is translucent with a slight yellow color, while the CTS/PRDQA membrane (1:0.5 in mass) presents deep yellow, opaque and relatively rough surface. This may be caused by the fact that after blending with PRDQA, some interactions exist that may result in the formation of 3D network structures between CTS and PRDQA molecules and the compatibility of the system becomes worse. Figure 4b and 4c show the cross profile SEM pictures of the two membranes. From the picture of the pristine CTS membrane, we can see that the membrane is relatively homogeneous without obvious micro-voids. After blending with PRDQA, the cross profile becomes rough, and small shallow folded cavities are observed to be irregularly distributed in the membrane. PRDQA provides activate groups (quaternary ammonium groups) in the polymer matrix but also accounts for the phase separation in the membrane.

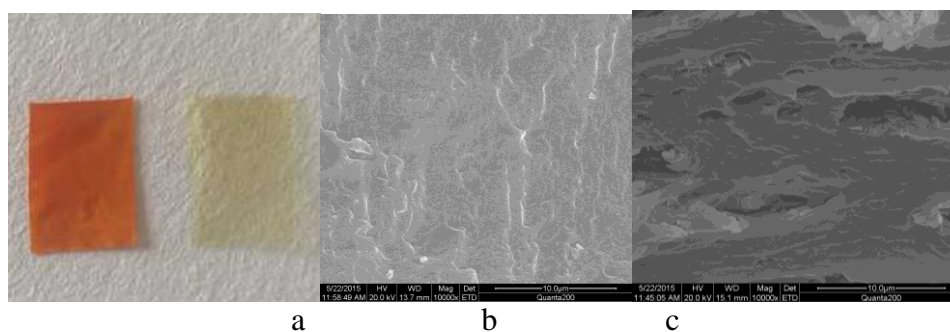


Figure 4. The digital photograph and cross profile SEM pictures of the pristine CTS membrane and the CTS/PRDQA membrane. a. the digital photograph, b. the cross profile SEM picture of the pristine CTS membrane, c. the cross profile SEM picture of the CTS/PRDQA membrane.

On the other hand, the structure of the CTS/PRDQA membrane becomes relatively loose due to the formation of these small shallow folded cavities and more water molecules/charge carriers could be retained, which are beneficial to the improvement of both membrane's conductivity and flexibility..

3.3 Thermal analysis

Thermal stability of the pristine CTS membrane and the CTS/PRDQA membrane (1:0.5 in mass) was investigated by thermo gravimetric analysis (TGA) from 25°C to 650°C under air atmosphere. The weight loss curves are shown in Figure.5.

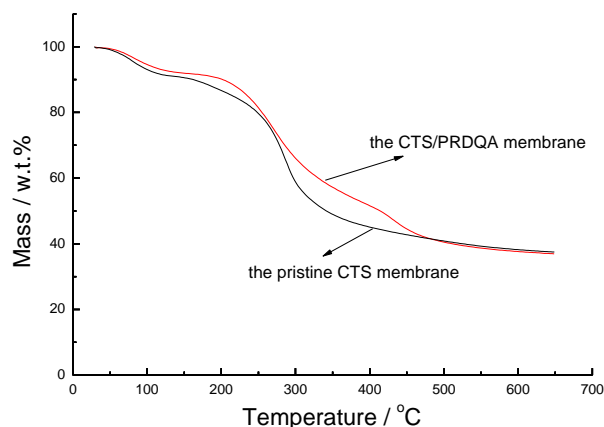


Figure 5. TGA profile of the pristine CTS membrane and the CTS/PRDQA membrane.

Table 1. TGA data of the pristine CTS membrane and the CTS/PRDQA membrane.

Membrane	T_{10} (°C)	T_{IDT} (°C)	T_{50} (°C)	T_{max} (°C)	Char yield (%)
the pristine CTS membrane	161	138	342	285	37.46
the CTS/PRDQA membrane	202	158	414	281	36.93

The characteristic data (T_{10} , T_{IDT} , T_{50} , T_{max} and char yield) are listed in Table 1. T_{max} represents the temperature of maximum speed on weight loss and T_{IDT} is the initial decomposition temperature of the second stage. T_{10} and T_{50} refer to the temperatures of 10% and 50% weight loss, respectively. Similar to other reported alkaline membranes [4, 29, 39], the initial weight loss of the membranes (30–160°C) mainly belongs to the removal of water molecules from the polymer matrix or the moisture from the air. Some differences between the pristine CTS membrane and the CTS/PRDQA membrane in the weight loss process were observed. First, the former shows a stage in the temperature range of 160 to 500°C, which is attributed to the oxidative degradation of the CTS main chain. However, the later shows two stages instead. The stage in the range of 160 to 360°C is assigned to the oxidative decomposition of quaternary ammonium groups, the destruction of cross-linking bridge between the two polymer backbones as well as the initial oxidative degradation of CTS and PRDQA, while the other stage up to 500°C is due to the further oxidative degradation of CTS and PRDQA.

As shown in Table 1, T_{IDT} of the pristine CTS membrane is 138°C, but after blended with PRDQA, this value increases to 158°C. This improvement of the thermal stability of the CTS/PRDQA

membrane assures the fuel cell operation under 100°C possible. It is also observed that the weight loss curve for the CTS/PRDQA membrane drops slower than that of the pristine CTS membrane, indicating that heat release is dramatically reduced. Furthermore, the T_{10} , T_{50} and T_{max} temperatures of the CTS/PRDQA membrane are 202°C, 414°C and 281°C respectively, which are higher than or comparable to those of the pristine CTS membrane (161°C, 342°C and 285°C). This improved thermal stability may be due to the covalent bonds and the intra- or inter-molecular hydrogen-bonds of the CTS/PRDQA membrane. The network structures formed in the CTS/PRDQA membrane contribute to the thermal stability enhancement [40, 41].

3.4 Mechanical properties

The mechanical property of CTS/PRDQA composite membranes was evaluated by the tensile strength and tensile elongation, and the results are presented in Table 2.

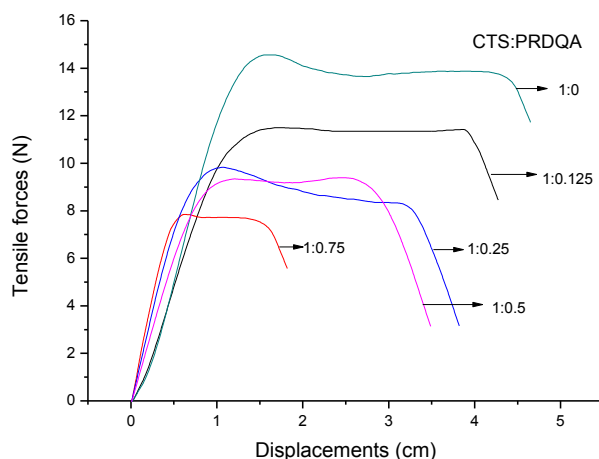


Figure 6. Stress-strain curves of the CTS/PRDQA composite membranes.

Table 2. The mechanical property of the CTS/PRDQA composite membranes. ($t = 30 \pm 2^\circ\text{C}$).

CTS/ PRDQA (by mass)	1:0	1:0.12 5	1:0.25	1:0.5	1:0.75	CS/EMIm C-Co-EP- OH ⁻ 1:0.5[39]	CS/EMIm C-Co-EP- OH ⁻ 1:0.75[39]	Semi- IPN- 21% [40]	Semi- IPN- 38% [40]
TS (MPa)	24.1 7	20.17	17.45	16.6	14.08	26.95	1.68	20	17.5
E_b (%)	8.56	7.84	6.40	5.20	3.10	6.72	1.57	8.1	3.3

Figure.6 illustrates the typical stress–strain curves in order to further clarify the effects of dyeing, grafting and crosslinking behaviors on the mechanical property of the membranes. It can be seen that the tensile strength values are in the range of 24.17-14.08MPa, and the tensile elongation values are in the range of 8.56-3.10%. The CTS/PRDQA membranes at low content of PRDQA (CTS/PRDQA = 1:0.125 by mass) show a high tensile strength, i.e., 20.17MPa, and an elongation at break of 7.84%, these are comparable to some CTS-based membranes [39-41] reported elsewhere. With increase of the content of PRDQA in the membranes, the tensile strength of the CTS/PRDQA membranes decreased significantly. This may be due to two factors: firstly, the phase separation phenomena becomes stronger when the content of PRDQA is higher in the membranes; secondly, since PRDQA can form more than two covalent bonds with CTS macromolecules, when the degree of cross-linking between CTS and PRDQA increases, the relative movement of CTS chains becomes more restricted, and there is less opportunity for chain motion to help equalize the distribution of stress on individual chains, which leads to stress concentration, so the breaking strength decreases [42]. The results show that this kind of membrane can withstand the stress during MEA assembly in a fuel cell test, as shown in the following section.

3.5 The ion exchange capacity

The ion exchange capacity (IEC) of the polymer membrane is closely related to the OH^- conductivity, which plays a key role on the membrane performance. From the data shown in Table 3, it can be seen that the IEC values of the prepared CTS/PRDQA membranes are in the range of 0.41-1.24mequiv g^{-1} . With the increase of the content of PRDQA (CTS/PRDQA in mass, from 1:0.125 to 1:0.75), the IEC values increase. This can be explained by the fact that with the increase of the content of PRDQA, the quaternized ammonia groups increase, and thus the charge carriers OH^- increase. Furthermore, the structure of membrane becomes relatively loose with the increasing of the content of PRDQA in the membrane.

Table 3. Physical-chemical properties of CTS/PRDQA at room temperature

CTS/PRDQA (by mass)	WU (g g^{-1})	σ ($\times 10^{-3}\text{S cm}^{-1}$)	Swelling ratio		IEC (mequiv g^{-1})
			$\Delta S/S$ (%)	$\Delta V/V$ (%)	
1:0.125	0.82	2.15	41.65	81.17	0.41
1:0.25	0.73	3.92	33.93	73.89	0.65
1:05	0.67	8.17	24.44	65.42	1.08
1:0.75	0.62	9.09	21.52	49.69	1.24

This may, on the other hand, provide more OH^- groups that can enter into the internal structure of the membrane during the ion-exchange process.

3.6 Water uptake and swelling ratio

One of the key parameters that need to pay attention in the development of alkaline polymer exchange membranes is water uptake (WU). Either the ionic hopping conduction mechanism or the ionic diffusion/vehicular conduction mechanism in the membrane is related to the water content. The former is performed by the bound water and the latter is done by the free water [43]. In general, water cluster can offer transport channels for OH^- inside the membrane, however, too much water inside the membrane will have negative effects on OH^- conductivity (dilution effect). For example, it will decrease the dimensional stability of the membranes, lead to high permeability, increase the membrane's fragility and even make the membranes soluble in hot water [44]. For a real application in fuel cells, the membranes' water uptake should be optimized in terms of both ionic conductivity and mechanical properties.

Table 3 shows a typical effect of different contents of PRDQA on water uptake and swelling ratio of CTS/PRDQA membranes. It is found that water uptake of the membranes falls in the range of 0.62-0.82 g g⁻¹ and decreases gradually with the increasing content of PDRQA. This might be due to two factors: firstly, a significant increase in the network formation within the membrane can be achieved by increasing the content of PRDQA, since the crosslinking reactions take place in CST with the addition of PRDQA, and the formed network via reactions will suppress membranes' swelling effectively. Secondly, hydrophilic groups such as -OH and -NH₂ in the CTS macromolecular reduce as the reaction progresses. However, the water uptake of the membranes doesn't decline dramatically, and the minimum value of the water uptake, i.e., 0.62 g g⁻¹ in this work, can offer enough channels to transport, because the quaternized chitosan can readily absorb water due to the introduction of the hydrophilic quaternary ammonium sites [40, 45]. Thus the water uptake of CTS/PRDQA membranes could be simultaneously tailored by fine tuning the crosslinking density of the membrane as well as the hydrophilic performance of the introduced groups. The former functions seem to play more important role in the membrane based on CTS matrix [41]. By controlling the parameters as explained above, it is found that water uptake of CTS/PRDQA membranes could be well controlled to an optimized range, which has the advantages over some other CTS based membranes [39-41] and other polymer based membranes claimed in the literatures [4,29].

On the other hand, the swelling property is another critical factor that affects the performance of the ionic exchange membranes such as dimensional stability, resistance of the membranes due to the increased thickness and easy migration of ions inside the membranes [46]. In Table 3, the swelling ratio (SR) for CTS/PRDQA alkaline anion-exchange membranes at room temperature is illustrated to evaluate the dimensional stability of the membranes. It can be observed that SR of the CTS/PRDQA membranes decreases gradually with the increasing content of PDRQA. This can be explained that the membrane containing higher content of PRDQA has lower free volume due to high dense cross-linkages in the matrix and stronger hydrogen-bonding effect between CTS and PRDQA molecules. As

shown in Table 3, the change difference in length due to swelling is also observed, i.e., relatively small change of about 21.52-41.65% in area SR but large change of about 49.69-81.17% in volume VR , this is mainly due to the larger change in L_z direction. The relatively large change in L_z direction compared to those in L_x and L_y directions is acceptable to anion exchange membrane fuel cell application.

3.7 Ionic conductivity

After being hydrated for 2h at room temperature, the CTS/PRDQA membranes with different PRDQA contents were investigated by impedance spectroscopy for ionic conductivity measurement, and the results are presented in Table 3. The OH^- conductivity increases from $2.15 \times 10^{-3} \text{ S cm}^{-1}$ to $9.09 \times 10^{-3} \text{ S cm}^{-1}$ for CTS/PRDQA in a mass ratio of 1:0.125 and 1:0.75, respectively. This can be attributed to an increase in the number of charge carriers in the CTS/PRDQA membranes. These results are higher than other polymer based membranes such as quaternized epichlorhydrine polymer [47] and quaternized PVA which were prepared previously in our lab [4, 29], and are comparable to other CTS based membranes listed in the literature [39-41]. As shown in Table 3, it is also found that with a further increase of the content of PRDQA, the increase of the OH^- conductivity tends to level off. This may be due to the decreased water uptake, which affects the migration rate of ions inside the membrane. Deserved to be mentioned here, after initial ion exchange of the membrane to the hydroxide form, the hydroxyl ions are neutralized quickly and may converted from OH^- to HCO_3^- form during the exposure to the air, which leads to the decrease of the conductivity of the membranes. It is expected that the conductivities of the CTS/PRDQA membranes should be higher if only OH^- ions exist.

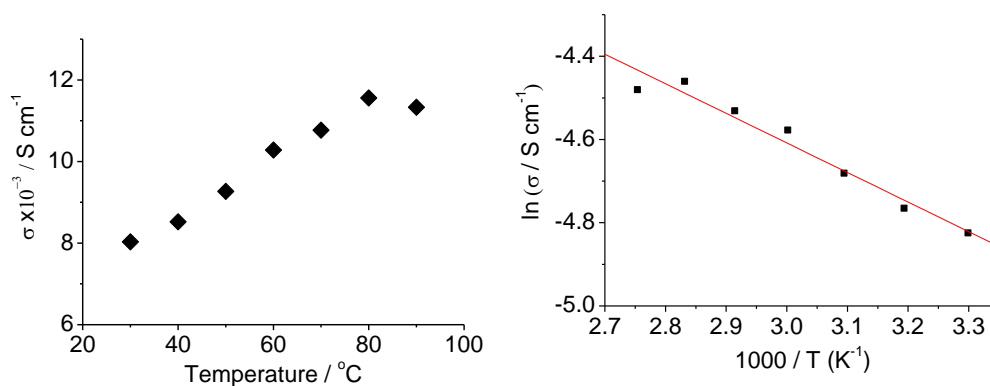


Figure 7. a. Temperature dependence of OH^- conductivity, b. The $\ln\sigma$ vs. $1000/T$ plot for CTS/PRDQA alkaline membranes.

Figure.7 shows the temperature dependence of the OH^- conductivity of the CTS/PRDQA membranes (1:0.5 in mass). The membranes exhibit positive temperature-conductivity dependencies in the tested temperature range from 30°C up to 80°C . This is due to the enhanced thermal mobility of OH^- in the membranes at elevated temperatures. Furthermore, the polymeric main chains will provide a larger free space favoring the ion transport at elevated temperatures [48]. With a further increase of

the temperature to 90°C, the OH^- conductivity slightly decreases, which might be caused by the Hofmann degradation and nucleophilic substitution of the quaternary ammonium group at an elevated temperature. The apparent activation energy for ion-migration, E_a , is estimated from Figure.7b. Linear regression of $\ln\sigma$ vs. $1000/T$ was performed assuming an Arrhenius relationship. The ion transport activation energy, E_a , derived from the slopes of the Arrhenius plots, is ~ 5.91 kJ mol $^{-1}$, indicating that both the Grotthus mechanism and Vehicle mechanism co-exist in the membranes but with the former as the dominant part [49].

3.8 Alkaline resistance stability

Alkaline resistance stability of the membrane is recognized as a key factor that affects the electrochemical performance application, especially in high pH environment such as alkaline fuel cells and at elevated temperatures [4, 23, 29, 30, 50-52].

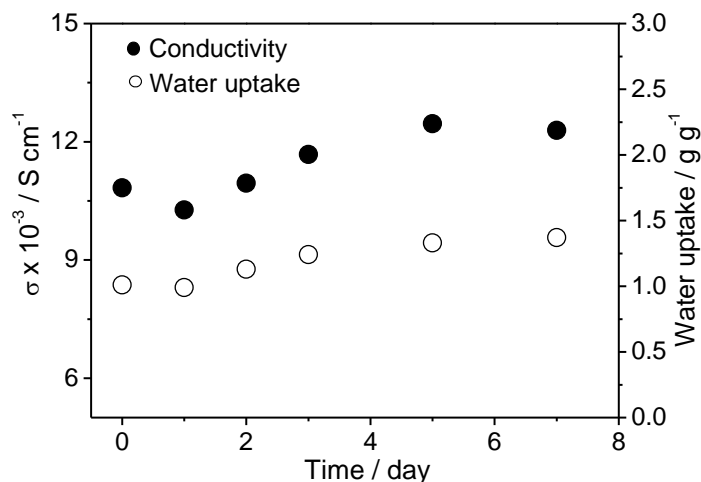


Figure 8. Time course of WU and OH^- conductivity of CTS/PRDQA alkaline membranes (1:0.5 in mass) in 8.0 M KOH solution at 80°C.

In Figure.8, the alkaline resistance stability of CTS/PRDQA alkaline membranes (1:0.5 in mass) was investigated by immersing the membranes into hot KOH solutions (8M) at 80°C for seven days. After complete removal of the free KOH from the membrane surface, the OH^- conductivity and water uptake of the membranes were determined. As shown in Figure.8, the OH^- conductivity slightly decreases at first and then increases to 12.46×10^{-3} S cm $^{-1}$. The reason why the OH^- conductivity goes down at first is due to the well-known Hoffman degradation and nucleophilic substitution reaction that cause the reduction of some exposed quaternary ammonium groups. However, further reaction is suppressed by the formed network structure between CTS and PRDQA. Moreover, the membranes were swelled due to long time soaking, the increased water content facilitated the mobility of OH^- , and more KOH could be doped into the micro structures of the membranes. The above factors

result in an increase in the conductivity of the CTS/PRDQA membrane. In terms of the water uptake, it presents a trend of rising as a whole, that alkali lye gradually penetrates into the membrane is one reason, the other is because alkali lye can cause the hydrolysis of some covalent bonds and thus reduce the network structure formed between CTS and PRDQA. In summary, the results show that the CTS/PRDQA membranes process good alkaline stability and can withstand OH^- attack in a real fuel cell operation.

3.9 Single-cell performance

The membrane electrode assembly (MEA) is one of the core components affecting the overall performance of PEM fuel cells. Cell performances using CTS/PRDQA (1:0.5 by mass) membrane based MEA in H_2/O_2 mode were measured at room temperature. As shown in Figure.9, the CTS/PRDQA membrane based single cell shows that the open-circuit voltage (OCV) is around 991.6mV and the peak power density is around $29.1mW\ cm^{-2}$ at current density of $57.4mA\ cm^{-2}$, respectively. These values are comparable to Quaternized-chitosan membranes ($\sim 23mW\ cm^{-2}$ at $50^\circ C$) [53], CS/EMImC-Co-EP- OH^- membranes ($21.7mW\ cm^{-2}$ at room temperature) [39] and PVA/PDDA alkaline anion-exchange membranes ($35.1mW\ cm^{-2}$ at room temperature) [30], respectively, and even higher than those of PVA/ TiO_2 composite membrane ($7.54mW\ cm^{-2}$ at $60^\circ C$) [54] and QPVA/Q- SiO_2 membrane ($0.27mW\ cm^{-2}$ at room temperature) [55]. However, the CTS/PRDQA membrane shows much lower cell performance than the Nafion[®] membranes.

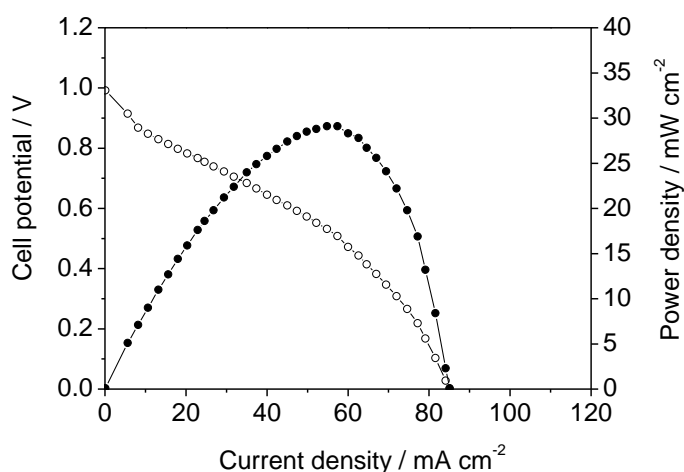


Figure 9. Polarization curves and power densities of the CTS/PRDQA membrane (1:0.5 in mass) in H_2/O_2 mode at room temperature.

This can be explained by two factors: (1) the ionic conductivity of the membrane is not as high as Nafion membranes; and (2) since the cell performance is also affected by many other factors such as catalysts and the MEA fabrication procedures. CTS/PRDQA membranes are very different from the fluoropolymer anion exchange membranes where a good three phase boundary could be achieved

among the membrane, catalyst and the gas diffusion electrode (GDE), and thus the ion transfer between the CTS/PRDQA membrane and Nafion-based catalyst layer is not good. Further improvements in the performance of MEA testing are expected through optimizing MEA fabrication techniques, binders for the membranes as well as the catalyst loading.

4. CONCLUSIONS

In this work, novel alkaline anion-exchange membranes from CTS/PRDQA composites have been prepared using combined blending and dyeing procedures. Studies on FT-IR spectroscopy showed that PRDQA was successfully introduced into the polymer matrix. The micro morphologies of the membranes were investigated using SEM micrograph. Both studies proved that the membranes possessed the capability to conduct OH^- . The investigation of thermal degradation behaviors by TGA for the pristine CTS membrane and the CTS/PRDQA membrane (1:0.5 by mass) revealed that the addition of dye stuff enhanced the thermal stability of the membrane at high temperature due to the formed network structure. The resulting membranes exhibited the conductivities of 2.15×10^{-3} , 3.92×10^{-3} , 8.17×10^{-3} and $9.09 \times 10^{-3} \text{ S cm}^{-1}$, respectively at room temperature with the increasing of the content of PRDQA in the membranes. The OH^- conductivity of the membranes was found to increase with the increase of the temperatures up to 80°C and then slightly went down at 90°C . The strong alkaline resistance stability of the membranes was proved in 8.0M of KOH at 80°C without any loss of both integrity and OH^- conducting behavior during one week of evaluation. A preliminary fuel cell test using CTS/PRDQA (1:0.5 by mass) alkaline membrane in H_2/O_2 mode showed a peak power density of 29.1 mW cm^{-2} at the current density of 57.4 mA cm^{-2} and the OCV was found to have 991.6 mV at room temperature. All of the promising results suggested that the CTS/PRDQA membranes could be new candidates for alkaline PEM fuel cell applications. In the future, we will have a further study in the areas such as synthesis or selection of the polymeric reactive dyes, optimization of the membrane preparation process, addition of plasticizer as well as the optimization of hot pressing procedures (temperature and pressure) to promote this technological innovation.

ACKNOWLEDGEMENTS

This work was financially supported by Industry-Academia-Research Joint Innovation Fund of Jiangsu Province (BY2015057-06) and the Nature Science Foundation of Jiangsu Province (BK20141261). Great thanks to Donghua university, Yancheng institute of technology, Jiangsu zhongzhan vehicle accessories Co.LTD, Wujiang taoyuan dyestuff Co.,Ltd and Yancheng dyeing and printing Co.LTD for offering some chemicals and funding generously. All financial support is gratefully acknowledged.

References

1. G. Couture, A. Alaaeddine, F. Boschet, B. Ameduri, *Prog. Polym. Sci.*, 36(2011) 1521-1557.
2. X.Zhang, J.Chen, *J. Power. Sources.*, 196(2011)10088-10093.
3. T.Xu, Z.Liu, W.Yang, *J. Membr. Sci.*, 249(2005)183-191.

4. T.C.Zhou, J.Zhang, J.L.Qiao, L.L.Liu, G.P.Jiang, J.Zhang, Y.Y.Liu, *J. Power Sources.*, 227(2013)291-299.
5. G.Li, J.Xie, H.F.Cai, J.L.Qiao, *Int. J. Hydrogen Energy.*, 39(2014)2639-2648.
6. V.Neburchilov, J.Martin, H.Wang, J.Zhang, *J. Power Sources.*, 169(2007)221-238.
7. K.Kai, H.K.Phil, C.N.Young, *J. Appl. Polym. Sci.*, 99(2006)1415-1428.
8. S.R.Samms, S.Wasmus, R.F.Savinell, *J. Electrochem. Soc.*, 143(1996) 1225-1232.
9. S.Sharma, B.G.Pollet, *J. Power. Sources.*, 208(2012)96-119.
10. M.Mamlouk, S.M.S.Kumar, P.Gouerec, K.Scott, *J. Power. Sources.*, 196(2011) 7594-7600.
11. M.Piana, M.Boccia, A.Filipi, E.Flammia, H.A.Miller, M.Orsini. *J. Power. Sources.*, 195(2010)5875-5881.
12. Z.Mohammad, A.G.Hubert, P.Michele, C.Stefano, *Int. J. Hydrogen Energy.*, 36(2011)5110-5116.
13. A.Ilie, M.Simoes, S.Baranton, C.Coutanceau, S.Martemianov, *J. Power. Sources.*, 196(2011)4965-4971.
14. G.Wang, Y.Weng, D.Chu, R.Chen, D.Xie, *J. Membr. Sci.*, 332(2009)63-68.
15. G.Wang, Y.Weng, J.Zhao, D.Chu, D.Xie, R.Chen, *Polym. Advan. Technol.*, 21(2010)554-560.
16. J.Ran, L.Wu, J.R.Varcoe, A.L.Ong, S.D.Poynton, T.Xu, *J. Membr. Sci.*, 415(2012)242-249.
17. Y.Xiong, J.Fang, Q.H.Zeng, Q.L.Liu, *J. Membr. Sci.*, 311(2008)319-325.
18. S.Huo, H.Deng, Y.Chang, K.Jiao, *Int. J. Hydrogen Energy.*, 37(2012)18389- 18402.
19. Y.Wang, J.L.Qiao, R.Baker, J.J.Zhang, *Chem. Soc. Rev.*, 42(2013)5768-5787.
20. T.N.Danks, R.C.T.Slade, J.R.Varcoe, *J. Mater. Chem.*, 13(2003)712-721.
21. H.Herman, R.C.T.Slade, J.R.Varcoe. *J. Membr. Sci.*, 218(2003)147-163.
22. L.Li, Y.Wang, *J. Membr. Sci.*, 262(2005)1-4.
23. L.Wu, T.W.Xu, D.Wu, X.Zheng, *J. Membr. Sci.*, 310(2008)577-585.
24. J.R.Varcoe, R.C.T.Slade, E.L.H.Yee, S.D.Poynton, D.J.Driscoll, D.C.Apperley, *Chem. Mater.*, 19(2007)2686-2693.
25. H.Liu, S.H.Yang, S.L.Wang, J.Fang, L.H.Jiang, G.Q.Sun, *J. Membr. Sci.*, 369(2011)277-283.
26. M.Mamlouk, J.A.Horsfall, C.Williams, K.Scott, *Int. J. Hydrogen Energy.*, 37(2012) 11912-11920.
27. M. Mamlouk, K. Scott, *J. Power. Sources.*, 211(2012)140-146.
28. T.A.Sherazi, J.Y.Sohn, Y.M.Lee, M.D.Guiver, *J. Membr. Sci.*, 441(2013)148-157.
29. T.C.Zhou, J.Zhang, J.Fu, G.P.Jiang, J.Zhang, J.L.Qiao, *Synth. Met.*, 167(2013) 43-50.
30. J.Zhang, T.C.Zhou, J.L.Qiao, Y.Y.Liu, J.J.Zhang, *Electrochim. Acta.*, 111(2013) 351-358.
31. Y.Zhao, J.Pan, H.M.Yu, D.L.Yang, J.Li, L.Zhuang, Z.G.Shao, B.L.Yi, *Int. J. Hydrogen Energy.*, 38(2013)1983-1987.
32. J.Fang, P.K.Shen, *J. Membr. Sci.*, 285(2006)317-322.
33. J.Hu, C.X.Zhang, J.Cong, H.Toyoda, M.Nagatsu, Y.D.Meng, *J. Power. Sources.*, 196(2011)4483-4490.
34. J.Zhou, M.Ünlü, I.Anestis-Richard, P.A.Kohl, *J. Membr. Sci.*, 350(2010)286-292.
35. S.Lu, J.Pan, A.Huang, L.Zhuang, J.Lu, *Fuel. Cell.*, 2(2009)6-11.
36. S.S.Alias, Z.M.Ariff, A.A.Mohamad, *Ceramics. International.*, 41(2015)5484- 5491.
37. Y.H.Li, C.Y.Cheng, N.K.Wang, H.Y.Tan, Y.J.Tsai, C.H.Hsiao, D.H.K.Ma, L.K.Yeh, *Colloids Surf., B*, 126(2015)237-244.
38. J.D.Daniel, D.G.Richard, E.W.Robert, *J.Am.Chem.Soc.*, 98(1976)5996-6000.
39. F.F.Song, Y.S.Fu, Y.Gao, J.D.Li, J.L.Qiao, X.D.Zhou, Y.Y.Liu, *Electrochimica. Acta.*, 2015 in press.
40. J.L.Wang, R.H.He, Q.T.Che, *J. Colloid Interface Sci.*, 361(2011)219-225.
41. W.Ying, P.Brant, A.M.C.Katherine, V.T.Buia, *J. Power. Sources.*, 195(2010)3785- 3793
42. T.C.Zhou, X.M.He, C.Guo, J.Yu, D.L.Lu, Q.Yang, *Text.Res.J.*, 85(2015)701-708.
43. K.D.Kreuer, S.J.Paddison, E.Spohr, M.T.Schuster, *Chem. Rev.*, 104(2004)4637- 4678.
44. T.C.Zhou, R.Shao, S.Chen, X.M.He, J.L.Qiao, J.J.Zhang, *J. Power. Sources.*, 293(2015)946-975.
45. Y.Xiong, Q.L.Liu, Q.G.Zhang, A.M.Zhu, *J. Power. Sources.*, 183(2008)447-453.

46. J.A.Kerres, *Fuel. Cells.*, 5(2005)230-245.
47. E.Agel, J.Bouet, J.F.Fauvarque, *J. Power. Sources.*, 101(2001)267–274.
48. B.C.Lin, L.H.Qiu, J.M.Lu, F.Yan, *Chem. Mater.*, 22(2010)6718-6725.
49. Q.Hu, Y.Shang, Y.Wang, *Int. J. Hydrogen Energy.*, 37(2012)12659-12665.
50. D.Stoica, L.Ogier, L.Akrour, F.Alloin, J.F.Fauvarque, *Electrochim Acta.*, 53(2007) 1596-1603.
51. J.M.Yang, H.Z.Wang, C.C.Yang, *J. Membr. Sci.*, 322(2008)74-80.
52. J.L.Qiao, J.Fu, L.L.Liu, Y.Y.Liu, J.W.Sheng, *Int. J. Hydrogen Energy.*, 37(2012) 4580-4589.
53. W.Ying, P.Brant, A.M.C.Katherine, V.T.Bui, H.Ela, *J. Power. Sources.*, 185(2008) 183–187.
54. C.C.Yang, S.S.Chiu, S.C.Kuo, T.H.Liou, *J. Power. Sources.*, 199(2012)37-45.
55. C.C.Yang, *J. Membr. Sci.* 288(2007)51-60.

© 2016 The Authors. Published by ESG (www.electrochemsci.org). This article is an open access article distributed under the terms and conditions of the Creative Commons Attribution license (<http://creativecommons.org/licenses/by/4.0/>).